Shaping of femtosecond pulses using phase-only filters designed by simulated annealing

A. M. Weiner

School of Electrical Engineering, Purdue University, West Lafayette, Indiana 47907-1285

S. Oudin and D. E. Leaird

Bellcore, 331 Newman Springs Road, Red Bank, New Jersey 07701-7040

D. H. Reitze

Lawrence Livermore National Laboratory, P.O. Box 808 L-251, Livermore, California 94550

Received August 20, 1992; accepted October 28, 1992; revised manuscript received November 30, 1992

We describe generation of shaped femtosecond waveforms by using frequency-domain phase-only filters designed by numerical optimization techniques. The task of filter design for pulse shaping in the time domain is directly analogous to the design of phase-only filters for beam shaping and array generation in the spatial domain. We experimentally tested phase filters that were designed to produce ultrafast square and triangle pulses and femtosecond pulse sequences. Our results demonstrate the ability to generate high-quality terahertz-repetition-rate sequences of femtosecond pulses by means of low-loss phase-only filtering. On the other hand, experiments that tested generation of individual shaped pulses, such as square pulses, were less successful than previous experiments that used simultaneous phase and amplitude filtering. Our results indicate the importance of building increased robustness against variations in the input pulse shape into the phase-only filter design.

1. INTRODUCTION

Substantial effort has been devoted to the design and fabrication of optical beam-splitting elements that transform single laser sources into two-dimensional arrays of optical beams for parallel optical computing systems and optical interconnect applications. A number of approaches for realizing such beam-splitting elements have been considered, including conventional multiple-exposure holographic techniques,[1] refractive[2] and Fresnel[3] lenslet arrays, and computer-designed phase-only filters placed at the Fourier plane of an optical system. One well-known example of a phase-only filter is the Dammann grating,[4–8] which is used to generate large, highly uniform beam arrays for digital optical computing systems. Other phase-only filter designs are used to produce multiple-beam arrays with arbitrary, nonuniform intensity ratios for neural-networks applications.[9] Salient points that are related to phase-only filters for array generation include the following: (a) the use of phase-only filtering allows for low loss and high efficiency; (b) the beam array in the output plane is determined by the Fourier transform of the spatial pattern on the filter; (c) usually only the intensity profile (and not the phase profile) of the output array is specified, which greatly increases the number of degrees of freedom available for filter design; (d) numerical optimization techniques are commonly used to synthesize filters with high efficiencies and desired intensity distributions.

In this paper we describe the use of numerical optimization techniques to design phase-only filters for creating specially shaped femtosecond pulses and pulse sequences. We have previously discussed synthesis of arbitrarily shaped, ultrafast temporal waveforms by phase and amplitude filtering of optical frequencies that are spatially dispersed within a simple grating and lens apparatus.[10,11] The resultant temporal pulse shape is given by the (one-dimensional) Fourier transform of the spatial pattern that is transferred from the phase and amplitude masks onto the spectrum. This is directly analogous to spatial beam shaping and array generation with the use of Fourier-plane filtering, in which the spatial output beam is the (two-dimensional) Fourier transform of the mask pattern. Therefore filter design techniques that are similar to those used for spatial beam shaping and array generation can also be used for synthesizing arbitrarily shaped femtosecond temporal signals.

In contrast to spatial array generation, in which only the output intensity profile is relevant, in femtosecond waveform synthesis both the temporal phase and the temporal intensity profiles are often specified. For example, in nonlinear propagation studies of dark-soliton pulses in optical fibers, soliton propagation was observed only when the shaped dark input pulses had both the proper phase and the proper amplitude signatures.[12] In other experiments, however, only the temporal intensity profile is important. One example that we investigated previously is femtosecond impulsive stimulated Raman scattering, in which timed sequences of femtosecond pulses were used to repetitively drive and selectively amplify optical phonons in solids.[13] Because the vibrational excitation depended only on the arrival time of the individual pulses within the sequence and not on the phase of the optical carrier wave,

0740-3232/93/051112-09$05.00

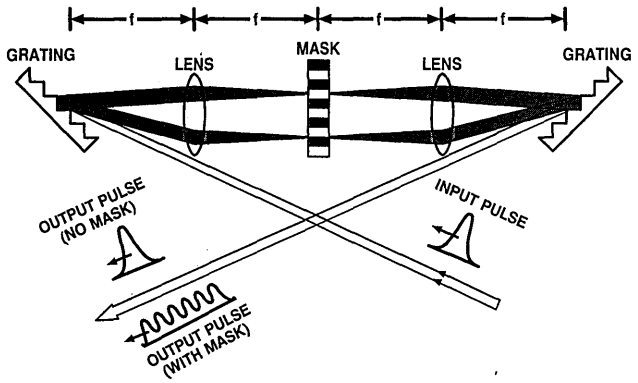

Fig. 1. Apparatus for shaping of femtosecond optical pulses.

we were able to use low-loss, phase-only filtering to produce the required femtosecond pulse sequence. In our investigations of phase-only filtering for femtosecond pulse shaping to date,[14] we considered only filter designs that were available analytically or by being borrowed from the literature on spatial array generation. Here we extend our previous research by using computer optimization techniques that are based on simulated annealing to design phase-only filters for more general femtosecond waveform synthesis. In particular, we report design, and experimental tests, of phase-only filters for generation of femtosecond square pulses and pulse sequences.

2. FEMTOSECOND PULSE SHAPING

The apparatus for femtosecond pulse shaping[11] is sketched in Fig. 1. Incident pulses with a duration of 75 fs at a wavelength of 620 nm are obtained from a colliding-pulse mode-locked ring dye laser.[15] The pulse-shaping setup consists of an identical pair of diffraction gratings placed at the outside focal planes of a unit-magnification confocal lens pair.[11,16] Spatially patterned masks are inserted midway between the lenses at the point where the optical spectral components experience maximal spatial separation. The second lens and grating reassemble the various spectral components into a single collimated beam. With no mask present inside the apparatus, the incident femtosecond pulse is transmitted without distortion. When patterned masks are present, the output pulse shape is given by the Fourier transform of the pattern transferred by the masks onto the spectrum. The temporal intensity profiles of the shaped pulses are measured by cross correlation by means of noncollinear second-harmonic generation, with the use of unshaped femtosecond pulses directly out of the colliding-pulse mode-locked laser as the reference. Note the similarity of this pulse-shaping apparatus to the well-known VanderLugt correlator.[17] The main difference is that our setup generates shaped temporal waveforms by utilizing the Fourier-transform relationship between time and optical frequency, whereas the VanderLugt correlator operates on spatially patterned beams through a two-dimensional spatial Fourier transform.

Pulse shaping is most conveniently understood in the frequency domain. The spectrum of the pulse emerging from the pulse-shaping setup is given by

$$E_{\text{out}}(\omega) = E_{\text{in}}(\omega)M_{\text{eff}}(\omega), \tag{1}$$

where $E_{\text{out}}(\omega)$ and $E_{\text{in}}(\omega)$ are the complex amplitudes of the output and the input electric-field spectra, respectively, and $M_{\text{eff}}(\omega)$ is the effective frequency filter implemented by the mask within the pulse-shaping setup.[18] $M_{\text{eff}}(\omega)$ is given by the complex transmittance of the physical mask $M(x)$ convolved with the spatial intensity profile of the focused beam:

$$M_{\text{eff}}(\omega) = \int \mathrm{d}x M(x)\exp[-2(x - \alpha\omega)^2/w_0^2]. \tag{2}$$

Here w_0 is the radius of the electric-field spatial profile of an individual frequency component at the masking plane and α denotes the spatial dispersion:

$$\alpha = \left(\frac{\mathrm{d}\omega}{\mathrm{d}x}\right)^{-1} = \frac{-\lambda^2}{2\pi c}\left(\frac{\mathrm{d}\lambda}{\mathrm{d}x}\right)^{-1}. \tag{3}$$

The spatial dispersion is determined by the angular dispersion of the grating and the focal length of the lens; for our setup, $\mathrm{d}\lambda/\mathrm{d}x = 2.95$ nm/mm and $\alpha = 6.92 \times 10^{-14}$ mm s. For a typical input pulse with a spectral width of the order of 10 nm, the spectral components are dispersed by several millimeters, and this sets the scale of the pulse-shaping masks. When the focused-laser spot size (typically 20 μm) is substantially smaller than the finest features on the mask (i.e., when the spectral resolution of the pulse-shaping setup exceeds that called for by the mask), the frequency filter is identical in form to the physical mask:

$$M_{\text{eff}}(\omega) \sim M(x/\alpha). \tag{4}$$

In this case the output pulse is given by the convolution of the electric-field profile of the input pulse with an impulse response function, which is simply a scaled version of the Fourier transform of the spatial pattern on the mask. On the other hand, when the physical mask contains features that are smaller than the spot size w_0, these smaller features will be smeared out by the convolution integral in Eq. (2). The effect in the time domain is to multiply the impulse response function by a Gaussian window function with width of the order of $3\alpha/w_0$ (~10 ps in the current setup). Thus the finite spectral resolution of the pulse-shaping apparatus will cause a roll-off of synthesized waveforms that extend over durations exceeding ~10 ps.

We used several approaches for realizing spatially patterned pulse-shaping masks. For most of the research reported in this paper, we utilize fixed masks that were fabricated by using standard photolithography.[11,19] Binary phase masks are fabricated on fused-silica substrates by reactive ion etching; for a π phase shift, an etch depth of $D = \lambda/2(n - 1) \approx 0.68$ μm is required. We sometimes use multielement (either 32 or 128 elements) liquid-crystal phase modulators instead of fixed masks.[20,21] By using a multielement modulator we can configure the phase pattern in real time and achieve gray-level phase control. Fixed-amplitude masks (not required for the current study) have been fabricated with gray-level control by patterned deposition of titanium–gold films on fused-silica substrates.[11,22] Finally, diffractive pulse-shaping masks that were fabricated by means of holographic recording have also been reported.[23,24]

To date, pure phase masking has been used for a number of pulse-shaping applications. Binary phase masks have been used to generate what have been called odd

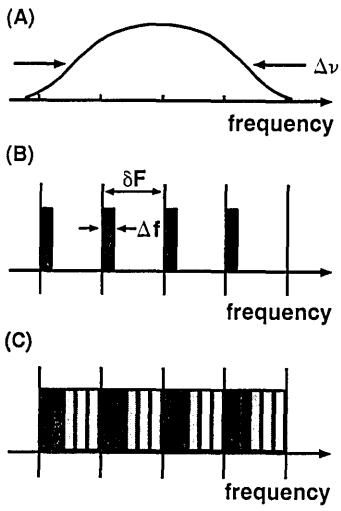

Fig. 2. Generation of high-rate pulse trains by spectral filtering: (A) input spectrum, (B) amplitude filter, (C) phase filter. For the phase filter, the various shaded rectangles denote different phases.

pulses[11] (pulse doublets in which the electric field is an antisymmetric function of time), coded pseudonoise bursts for spread-spectrum optical communications,[19] and terahertz-repetition-rate trains of femtosecond pulses for impulsive Raman-scattering studies.[13,14] Gray-level phase control by means of a multielement modulator has been used to achieve pulse-position modulation, to impart chirps onto ultrashort pulses, and to compress chirped pulses programmably.[20,21] Next we illustrate phase filtering by discussing generation of terahertz-rate pulse trains.

3. GENERATION OF TERAHERTZ-RATE PULSE TRAINS

The use of spectral filtering to produce high-rate pulse trains is shown schematically in Fig. 2.[14] We consider a single ultrashort input pulse with an optical spectrum as shown in Fig. 2(A). The bandwidth of the pulse is $\Delta\nu$, corresponding to an input pulse width of $\Delta\tau = 0.44/\Delta\nu$ (for a Gaussian pulse). The input pulse can be spread into a train of pulses by either amplitude filtering or phase filtering. In amplitude filtering, all but a periodically spaced set of frequencies are blocked. This results in a train of pulses, each of duration $\Delta\tau$, with a repetition rate that is equal to the frequency spacing δF. The number of pulses in the train is of the order of $\delta F/\Delta f$, where Δf is the spectral width of the individual passbands of the filter. Since the total transmission is only $\Delta f/\delta F$, the amplitude-filtering approach is inherently inefficient.

High-quality pulse trains can be generated without loss by use of a periodic phase-only filter, as depicted in Fig. 2(C). As in the case above, the repetition rate of the resulting pulse train is equal to the periodicity δF, but the envelope of the pulse train depends on the structure of the phase response within a single period. It can be shown that the output intensity profile $I(t)$ is equal to the Fourier transform of the autocorrelation of the filtered spectrum[14]:

$$I(t) = (1/2\pi)^2 \int d\Omega \exp(i\Omega t) \int d\omega E^*(\omega) E(\omega + \Omega). \quad (5)$$

Therefore, by using pseudorandom phase sequences with sharp autocorrelation peaks (such as those that are well known in spread-spectrum communications[25]) as the building blocks of the phase filter, one can generate pulse trains under a smooth envelope.

We have fabricated binary phase masks based on periodic repetitions of the so-called M (or maximal length) sequences.[25] Each period of the mask is divided into P pixels of width $\Delta f = \delta F/P$, with each pixel assigned a phase of either zero or $\Delta\varphi$, as determined by a particular M sequence. In the example considered here, we used a phase mask consisting of periodic repetitions of the M sequence {000100110101111}. The height of the central pulse in the train is sensitive to the phase difference $\Delta\varphi$ and is close to zero for $\Delta\varphi = \pi$; therefore we set $\Delta\varphi = 0.84\pi$, which for a length $P = 15$ maximal length sequence yields a central pulse with an amplitude matched to the smooth pulse-train envelope.

We have generated pulse trains at a variety of repetition rates by using a series of phase masks corresponding to different frequency periodicities δF. Measurements of pulse trains at 4.0- and 5.85-THz repetition rates are shown in Fig. 3.[14] The 4-THz pulse train shows a series of well-defined pulses under a smooth envelope. The fact that the minima between pulses do not completely reach zero is due mainly to the finite duration of the 75-fs probe pulses that we used to perform the cross-correlation measurement. For the higher-rate, 5.85-THz train, the envelope of the pulse sequence becomes somewhat irregular, and the contrast between individual pulses varies within the envelope. This degradation occurs when the individual pulses within the train begin to overlap. For pulse trains produced by phase filtering, the phase varies from pulse to pulse in a manner that is determined by the particular code; therefore interferences between neighboring pulses cause the observed irregularity. As the ratio of pulse duration to pulse separation decreases further, interferences between neighboring pulses become more severe, and the resulting pulse train becomes even more irregular. In the limit in which only one repetition of the phase code fits within the input spectrum, a pseudonoise burst rather than a pulse sequence is produced, as we have

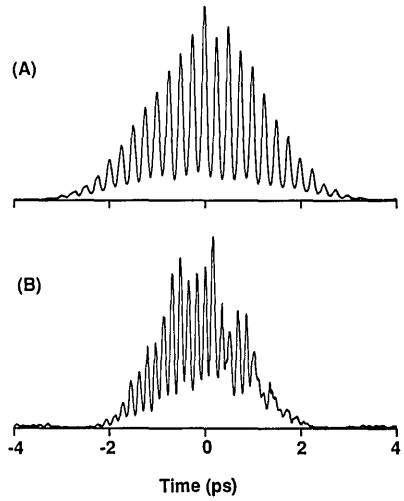

Fig. 3. Intensity cross-correlation measurements of (A) 4.0-THz, (B) 5.85-THz pulse trains produced by phase-only filtering. The phase difference was $\Delta\varphi = 0.84\pi$ for both traces.

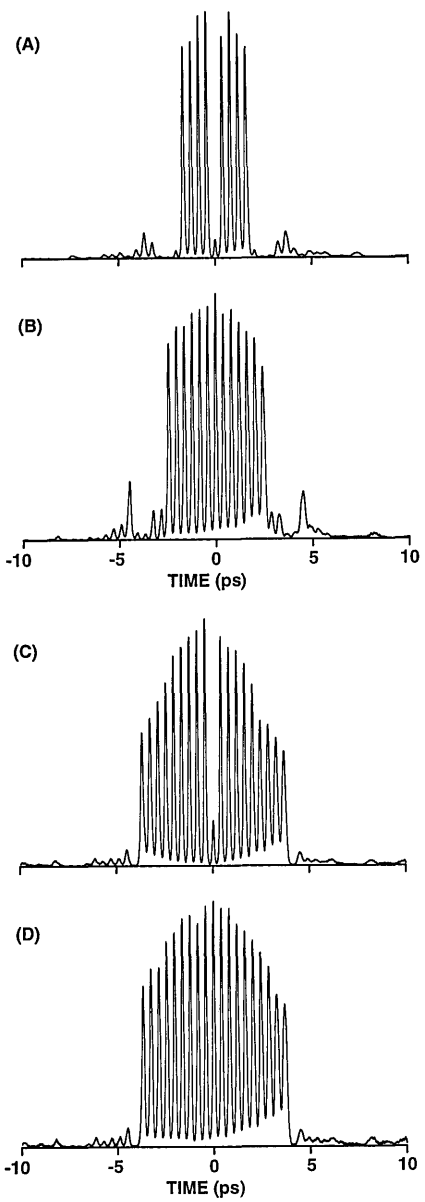

Fig. 4. Flat-topped pulse trains at a 2.5-THz repetition rate, produced by phase-only filters based on Dammann gratings. The phase difference was (A), (C) $\Delta\varphi = \pi$ and (B), (D) $\Delta\varphi = 0.85\pi$.

previously shown.[11,19] Of course, higher-repetition-rate pulse trains (to date, as high as 12 THz) can be achieved by using shorter input pulses.[26] Nevertheless, the irregularity that is observed when individual pulses do overlap will have an important bearing on synthesis of other waveforms, such as femtosecond square pulses (discussed below in Section 5).

Pulse trains with different envelopes can be generated by varying the details of the phase response within a single period. In general, a numerical optimization procedure is required for designing an appropriate phase filter for a specified output profile. However, pulse trains can also be generated by borrowing phase filters that were designed to serve as beam-splitting elements for optical interconnect systems. For example, flat-topped pulse trains can be generated by using filters based on the Dammann gratings[4–8] that were previously used to split an individual laser beam into an equally spaced, equal-intensity array of beams.

To demonstrate this point we fabricated a series of phase masks based on grating designs listed in Table 1 of Ref. 6, which we tested within a femtosecond pulse-shaping apparatus. Several examples of our data, showing femtosecond pulse trains at a 2.5-THz repetition rate, are shown in Fig. 4. Our results in the time domain are similar to those that were obtained previously in the spatial domain. All the traces exhibit a relatively uniform series of central pulses, with the intensity dropping off abruptly outside the central region. The different number of pulses—8, 13, and 18 in Figs. 4(A), 4(B), and 4(C), respectively—correspond to different Dammann-grating designs. The gratings that were used for Figs. 4(C) and 4(D) were identical except for the phase difference $\Delta\varphi$; consequently the resulting temporal profiles are also identical except for the amplitude of the central pulse, which depends sensitively on $\Delta\varphi$. The lack of perfect uniformity in the pulse amplitudes can be attributed to imperfections in the mask fabrication and to the finite spectral resolution of the pulse-shaping setup, which causes the regular roll-off observed at large times (see Section 2). The nearly equal-intensity central pulses account for ~80–85% of the total energy, with the remaining energy being distributed among various low-intensity sidelobes outside the central region. The observed 80–85% efficiency is consistent with the predicted efficiency of Dammann gratings. Note that, when one is using Dammann gratings as spatial beam-splitting elements, one can eliminate unwanted energy outside the central region simply by using a spatial aperture. In the time domain, however, implementation of the equivalent of an aperture that would eliminate the unwanted sidelobes is less straightforward.

4. DESIGN OF PULSE-SHAPING FILTERS BY SIMULATED ANNEALING

We used the simulated-annealing method developed by Metropolis and co-workers[27–29] to design phase-only filters for producing arbitrarily shaped, ultrafast temporal pulses. One begins by defining a cost (or energy) function C, which provides a measure of the deviation between the temporal pulse shape generated by the phase filter $M(\omega)$ that we wish to design and the target pulse $e_{\text{target}}(t)$. A series of partial cost functions C_i can be used to control different aspects of the generated waveform. The choice of the C_i is determined by the particular target waveform. For example, one partial cost function could seek to minimize the maximum deviation of the generated intensity from that of the target over a specific time interval as follows:

$$C_i = \text{Max}\left|\,|e(t)|^2 - |e_{\text{target}}(t)|^2\,\right|, \qquad |t| < T_0. \tag{6}$$

The generated field $e(t)$ is computed as

$$e(t) = \frac{1}{2\pi}\int \mathrm{d}\omega E_{\text{in}}(\omega)M(\omega)\exp(i\omega t), \tag{7}$$

where $E_{\text{in}}(\omega)$ is the input electric-field spectrum to the pulse shaper. The partial cost functions are weighted

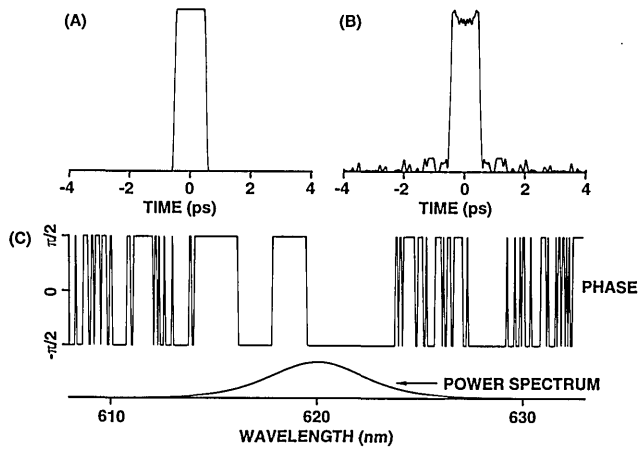

Fig. 5. Design of a phase-only filter for producing a 1.0-ps square pulse: (A) target intensity profile, (B) calculated intensity profile resulting from the phase-only filter, (C) phase filter designed by simulated annealing (top) and assumed input power spectrum (bottom). The phase filter was assumed to consist of 400 independent pixels.

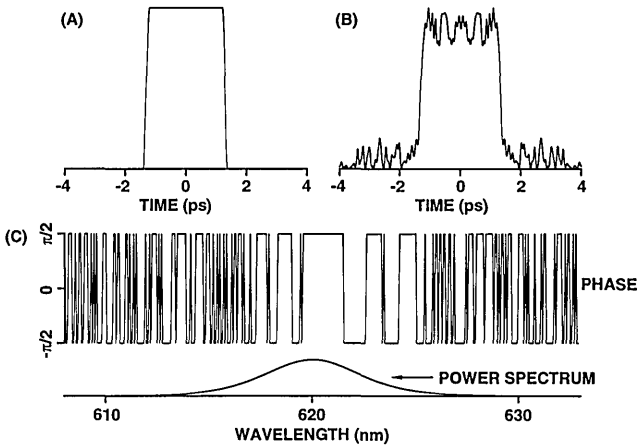

Fig. 6. Design of a phase-only filter for producing a 2.5-ps square pulse: (A) target intensity profile, (B) calculated intensity profile resulting from the phase-only filter, (C) phase filter designed by simulated annealing (top) and assumed input power spectrum (bottom). The phase filter was assumed to consist of 400 independent pixels.

and summed to give the total cost function

$$C = \sum w_i C_i . \tag{8}$$

The weights w_i can be chosen to permit optimization of specific features of the generated pulse; e.g., a large weight (penalty) could be assigned to minimize the amount of energy that resides outside a target interval.

We utilized simulated annealing to design phase filters for ultrafast square pulses, ultrafast triangle pulses, and femtosecond pulse sequences. We specify only the target intensity profile $|e_{\text{target}}(t)|^2$; the temporal phase is left unconstrained. We consider only binary phase filters with 0 and π phases; therefore the resulting output field satisfies $e(-t) = e^*(t)$, and the output intensity profiles are symmetric in time. Hence we compute the cost function only for $t \geq 0$. In our simulations we consider filters composed of various numbers of pixels, ranging from 128 pixels with a resolution of 0.092 THz/pixel (corresponding to the attributes of the 128-element liquid-crystal phase modulator[21]) to 400 pixels with a resolution of 0.05 THz/pixel (corresponding to the resolution achievable with fixed masks). We start with a phase filter in which each pixel is randomly and independently set to a phase of 0 or π. The minimization of C proceeds iteratively by flipping the phase of one randomly selected pixel at a time. The new $e(t)$ is calculated according to Eq. (6), and the change in the cost function ΔC resulting from the phase change is then evaluated. The new filter is always accepted if $\Delta C < 0$. For $\Delta C > 0$ the change is accepted with probability $\exp(-\Delta C/T)$, where T is a control parameter or temperature. By occasionally accepting a positive ΔC, one seeks to avoid settling into a local minimum of the cost function. One sets an annealing schedule by choosing an initial temperature and successively lowering the temperature after a prespecified number of iterations (or sometimes after a prespecified number of successful iterations). One chooses the initial temperature by computing differences between cost functions selected at random and setting T considerably larger than the largest ΔC that is encountered. In this way the probability of accepting a positive ΔC is initially greater, and the cost function is free to move about its entire parameter space and seek out the global minimum. We note that for a typical numerical design consisting of 400 individual pixels our simulations typically run from 15 to 30 min on a 600-kflop/s computer.

Typical simulation results for 1- and 2.5-ps-duration square target pulses are shown in Figs. 5 and 6, respectively. For these simulations the partial cost functions were (a) the maximum deviation along the (flat) top of the pulse, (b) the maximum deviation in the wings of the pulse, and (c) the amount of energy in the wings of the pulse. For the 1-ps-duration square pulse, the output pulse resulting from the optimized phase filter [Fig. 5(B)] closely resembles the target [Fig. 5(a)]. The intensity along the top of the pulse varies by ~10%, and the unwanted energy in the wings accounts for only ~15% of the total pulse energy. The phase profile of the optimized filter is shown in Fig. 5(C) along with the power spectrum of the assumed input pulse [in this case the input pulse is taken to be an ideal, 75-fs-duration, hyperbolic secant—$e(t) \sim \text{sech}(t/43\ fs)$—with the spectrum centered at

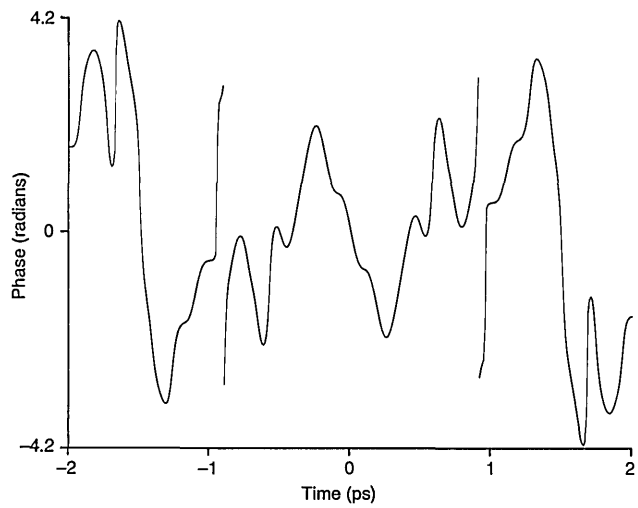

Fig. 7. Calculated phase profile of the square pulse from Fig. 5.

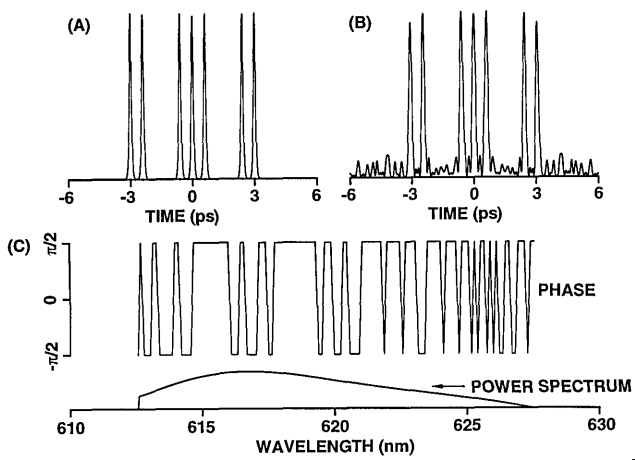

Fig. 8. Design of a phase-only filter for producing a femtosecond pulse sequence: (A) target intensity profile corresponding to a_n = {11001110011}, (B) calculated intensity profile resulting from the phase-only filter. (C) Phase filter designed by simulated annealing (top) and assumed input power spectrum (bottom). The phase filter was assumed to consist of 128 independent pixels, and the hard edge at 612.5 nm in the input power spectrum corresponds to the edge of the clear spectral window transmitted through the liquid-crystal modulator.

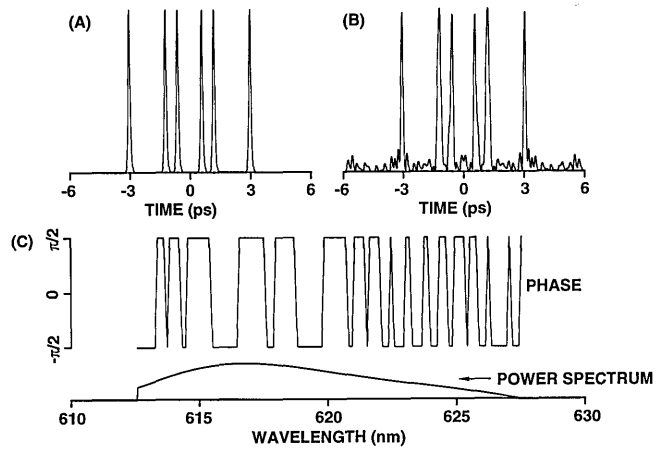

Fig. 9. Design of a phase-only filter for producing a femtosecond pulse sequence: (A) target intensity profile corresponding to a_n = {10011011001}, (B) calculated intensity profile resulting from the phase-only filter, (C) phase filter designed by simulated annealing (top) and assumed input power spectrum (bottom). The phase filter was assumed to consist of 128 independent pixels.

620 nm]. Note that the filter exhibits only a few phase changes in the 617–623-nm range, where most of the power spectrum lies. In the far wings of the spectrum, where the generated pulse shape is less sensitive to phase, many more changes in phase are seen to occur. Similar results can be observed in Fig. 6 for the case of a 2.5-ps square pulse. The maximum deviation along the top of the pulse in this case is ~25%, and ~27.5% of the input pulse energy resides within the target window. We performed many independent simulation runs with results comparable to those shown in the figures; the resultant square pulses are typically flat to within 10–25%, with ~15–30% of the total energy in the wings. The best results were generally achieved for the square pulses of shorter duration. Simulations that used slightly different cost functions, as well as those that used triangle target pulses, produced comparable results.

Figure 7 shows the calculated temporal phase profile of the 1-ps square pulse discussed in the previous paragraph. A significant phase variation is clearly evident, as expected: one requires a phase variation to account for the excess bandwidth because the pulse duration greatly exceeds the inverse bandwidth. Note that, although square pulses generated by using phase-only filters always exhibit a strong phase modulation, different phase-only filter designs resulting in similar temporal intensity profiles can lead to markedly different phase signatures. A time-domain phase variation is a principal difference between pulse shaping by phase-only filtering and pulse shaping by phase and amplitude filtering; in the latter case pulses with constant phase are possible.

We also used this procedure to design generalized Dammann gratings, i.e., phase filters that generate trains of pulses with equal amplitudes but unequal spacings. Again, the trains are necessarily symmetric in time because we consider only binary phase filters. For the simulations shown in Figs. 8 and 9, we used target pulse trains of the form

$$e_{\text{target}}(t) = \sum_n a_n u(t - nT), \tag{9}$$

where $u(t)$ represents a 75-fs pulse centered at time $t = 0$, T is the pulse spacing (500 fs in these examples), and a_n is either 0 or 1. Other pulse sequences, e.g., chirped sequences of pulses in which the pulse separation varies slightly from one pulse to the next, were also considered but are not discussed here. For the partial cost functions we used (a) the maximum deviation between the intensities of the individual peaks and the average peak intensity, (b) the deviations between the positions of each pulse in the train and the target positions, (c) the maximum intensity in the regions in which no energy is desired, and (d) the total energy not contributing to the desired target pulses. In addition, we used an asymmetric input spec-

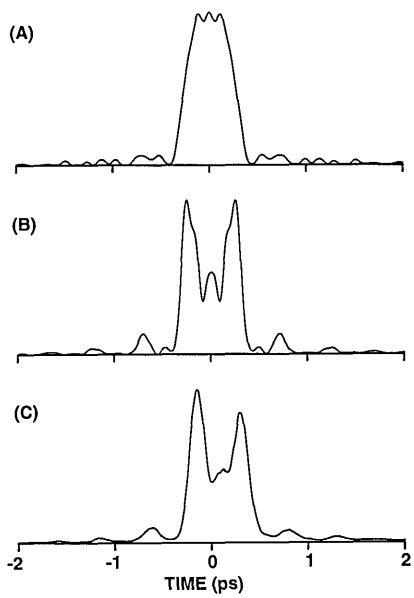

Fig. 10. (A) Calculated intensity profile resulting from a phase-only filter designed to transform a symmetric, sech(t) input pulse into a 0.5-ps square pulse, (B) calculated intensity profile resulting when the same phase-only filter is used with an actual laser spectrum, (C) measured intensity profile obtained by passing a femtosecond pulse through the pulse-shaping apparatus.

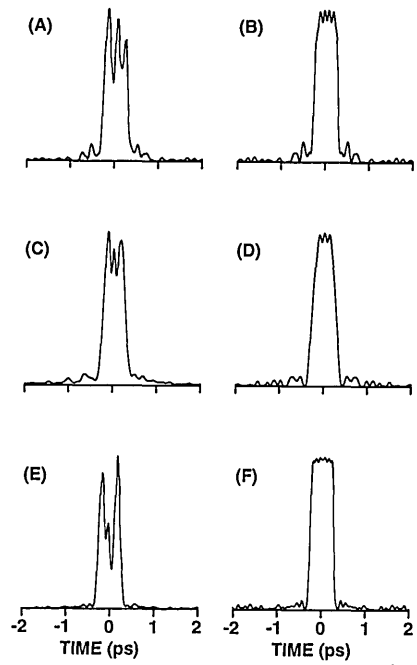

Fig. 11. Experimental tests of three different phase-only filters designed to produce 0.5-ps square pulses: (A), (C), (E) measured intensity profiles, (B), (D), (F) corresponding calculated intensity profiles. The phase filter consisted of (B), (D) 128 pixels, (F) 316 pixels. An actual laser power spectrum was used for (B), (F); a symmetric spectrum corresponding to sech(t) was used for (D).

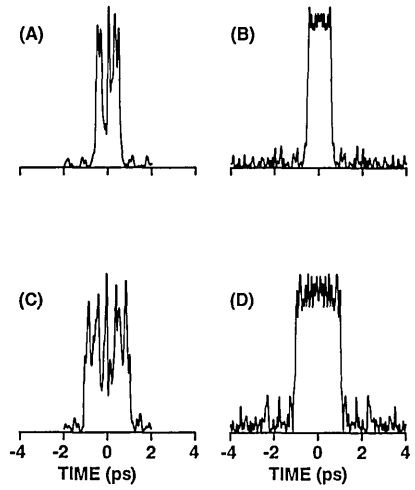

Fig. 12. Experimental tests of phase-only filters designed to produce ultrafast square pulses: (A) measured intensity profile for a 1-ps square pulse, (B) calculated intensity profile, (C) measured intensity profile for a 2-ps square pulse, (D) calculated intensity profile. The phase filters consisted of 316 pixels, and an actual laser power spectrum was used for the filter design.

trum, corresponding to the actual spectrum of our laser. Typical simulation results are shown in Figs. 8 and 9. Figures 8(A) and 9(A) display target pulse trains corresponding to the sequences $a_n = \{11001110011\}$ and {10011011001}, respectively. The pulse trains [Figs. 8(B) and 9(B)] that were generated by the optimized phase filters match the targets closely, particularly with respect to pulse position and uniformity of pulse height. One difference between the targets and the outputs, as is evident in Fig. 9, is the variation in the widths and shapes of the individual pulses. One could minimize this variation, in principle, by incorporating it as a constraint in the cost function. A loss of energy from the individual pulses to the regions between the pulses and in the wings is also evident. This typically accounted for ~30% of the input pulse energy. The optimized phase filters and the assumed input spectra are shown in Figs. 8(C) and 9(C).

5. EXPERIMENTAL RESULTS

We performed a number of femtosecond pulse-shaping experiments to test the phase-only filters that were designed by simulated annealing. Tests were performed for square pulses, triangle pulses, and pulse sequences, with the use of either fixed phase masks or the 128-element liquid-crystal phase modulator. Below we discuss our results on femtosecond square pulses.

We begin by discussing the effect of the laser input spectrum on the pulse-shaping results. Figure 10 shows the calculated output intensity profile that was produced from a filter designed to transform a sech(t) input pulse into a 0.5-ps square pulse. If the input is as assumed, a nice square pulse results [Fig. 10(A)]. On the other hand, as is evident in Figs. 8 and 9, the actual laser spectrum deviates from that of an ideal hyperbolic secant. If the identical phase filter is used for the calculation, together with the actual laser power spectrum (but still assuming a flat laser phase spectrum), the computed output pulse is severely affected [Fig. 10(B)]. We performed an experiment in which the multielement phase modulator was used to implement the phase filter. The measured intensity profile that was produced by the pulse-shaping apparatus [Fig. 10(C)] resembles the calculation [Fig. 10(B)]. This confirms the sensitivity of the pulse-shaping results to the input spectrum.

We tested a number of filter designs experimentally by fabricating phase-only masks by means of microlithography. Input pulses from the femtosecond dye laser were shaped with the use of these masks and were then measured. Figures 11 and 12 present a comparison of experimental and theoretical pulse shapes that are plotted for several square-pulse filter designs. Filters designed for a hyperbolic secant as well as for actual laser spectra

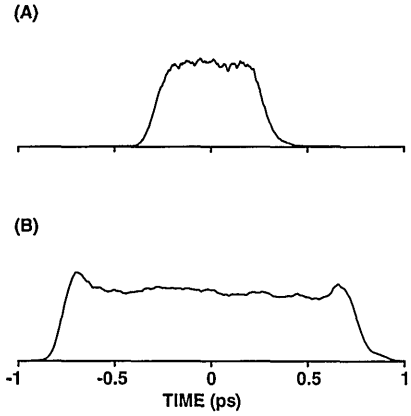

Fig. 13. Measured intensity profiles of ultrafast square pulses obtained by simultaneous phase and amplitude filtering: (A) 0.5-ps duration, (B) 1.5-ps duration. The smoothness of these intensity profiles is in contrast to those obtained by phase-only filtering.

were included. The data and theory show both similarities and differences. Similarities include the pulse durations, the abrupt turn-on and turn-off of the pulses, and the low amount of energy in the wings. The main difference is that the flatness of the experimental square pulses is usually degraded severely. This effect is even more pronounced for 1.0- and 2.5-ps square pulses than it is for 0.5-ps-duration pulses. Furthermore, the detailed structure that is present on the top of the measured square pulses varies noticeably from one filter to the next. Similar effects were observed for triangle pulses: although the energy always appears to be concentrated in the target region in time, the detailed experimental pulse shape varies from one filter to the next. These results are typical of data for ~40 phase filters that we fabricated.

Our results with square pulses produced by means of phase-only filters are in contrast to our previous results when we used phase and amplitude filters to generate ultrafast square pulses.[11,22,30] For comparison, Fig. 13 shows measurements of 0.5- and 1.5-ps square pulses that were obtained by using appropriate phase and amplitude filters within a pulse-shaping apparatus.[30] These pulses have sharp rising and falling transitions with little energy in the wings, and, in contrast to Figs. 11 and 12, here the tops of the square pulses are flat and essentially featureless.

We can understand these differences as follows. The output waveform produced by a pulse-shaping apparatus consists of the convolution of the input pulse with the impulse response function determined by the pulse-shaping masks. In the case of phase and amplitude filtering, the impulse response function has a square intensity profile and a constant phase profile. The convolution with the input pulse broadens the rising and falling edges of the output pulse but is not sensitive to the precise shape of the input pulse. On the other hand, the impulse response functions corresponding to the phase-only filters do not themselves have flat intensity profiles. Furthermore, their phase profiles vary dramatically in time (see, e.g., Fig. 7). The details of the impulse response function are sensitively balanced so that convolution with the assumed input pulse produces a flat temporal profile. We saw from Fig. 10 that the output pulse depends sensitively on the input pulse shape. Thus generation of square pulses with phase-only filters is not robust against changes in the input pulse shape. Although we did attempt to design phase-only filters that used a measured laser power spectrum, daily variations in the laser power spectrum make it difficult to design for the actual input pulse that will be used in experiments. Furthermore, even if the laser power spectrum were completely specified, complete specification of the input pulse for the filter design would require the making of additional, and rather involved, measurements to determine the phase profile of the input pulses.[31,32]

Finally, we contrast our square-pulse results with those reported in Section 3, in which we found that phase-only filters could be used to generate high-quality terahertz-rate trains of femtosecond pulses. The difference is that high-quality pulse trains [e.g., Fig. 3(A)] occur only when individual pulses in the train do not overlap, so that the variation in phase from pulse to pulse has no effect. The irregularity observed in square-pulse generation is analogous to the irregularity observed when the individual pulses in a pulse train begin to overlap [Fig. 3(B)]. Then the interferences between the individual pulses in the train do depend sensitively on the precise input pulse shape, and the pulse train develops an irregularity reminiscent of that observed in the square-pulse experiments.

6. SUMMARY

In summary, we have used numerical optimization techniques to design lossless phase-only filters for arbitrary femtosecond pulse shaping. Our pulse reshaping in the time domain is directly analogous to works on beam shaping and array generation with the use of phase-only filters in the spatial domain. We have experimentally tested filters designed to produce ultrafast square and triangle pulses as well as various sequences of femtosecond pulses. In all our designs the target intensity profile is specified, whereas the temporal phase profile is left unconstrained. Our measurements demonstrate the ability to generate high-quality, terahertz-repetition-rate sequences of femtosecond pulses, which closely resemble the target sequences. On the other hand, the flatness of ultrafast square pulses that are experimentally produced by phase-only filtering was degraded compared with ultrafast square pulses generated by simultaneous phase and amplitude filtering. Our results indicate the importance of building increased robustness against variations in the input pulse shape into the phase-only filter design.

S. Oudin is visiting from the Ecole Polytechnique, Palaiseau, France.

REFERENCES

1. D. Prongue and H. P. Herzig, "Design and fabrication of HOE for clock distribution in integrated circuits," presented at the Institute of Electrical Engineers Conference on Holographic Systems, Components, and Applications, Bath, UK, 1989.
2. M. C. Hutley, "Optical techniques for the generation of microlens arrays," J. Mod. Opt. **37,** 253–265 (1990).
3. K. M. Flood and J. M. Finlan, "Collimation of diode laser arrays using etched cylindrical computer generated holograms," in *Holographic Optics: Optically and Computer Generated,* I. Cindrich and S. H. Lee, eds., Proc. Soc. Photo-Opt. Instrum. Eng. **1052,** 186–190 (1989).
4. H. Dammann and K. Gortler, "High-efficiency in-line multiple imaging by means of multiple phase holograms," Opt. Commun. **3,** 312–315 (1971).
5. H. Dammann and E. Klotz, "Coherent optical generation and inspection of two-dimensional periodic structures," Opt. Acta **24,** 505–515 (1977).
6. U. Killat, G. Rabe, and W. Rave, "Binary phase gratings for star couplers with high splitting ratios," Fiber Integr. Opt. **4,** 159–167 (1982).
7. J. Turunen, A. Vasara, J. Westerholm, G. Jin, and A. Salin, "Optimization and fabrication of grating beamsplitters," J. Phys. D **21,** S102–S105 (1988).
8. J. Jahns, M. M. Downs, M. E. Prise, N. Streibl, and S. J. Walker, "Dammann gratings for laser beam shaping," Opt. Eng. **28,** 1267–1275 (1989).
9. M. P. Dames, R. J. Dowling, and D. Wood, "Efficient optical elements to generate intensity weighted spot arrays: design and fabrication," Appl. Opt. **30,** 2685–2691 (1991).
10. A. M. Weiner and J. P. Heritage, "Picosecond and femtosecond Fourier pulse shape synthesis," Rev. Phys. Appl. **22,** 1619–1628 (1987).
11. A. M. Weiner, J. P. Heritage, and E. M. Kirschner, "High resolution femtosecond pulse shaping," J. Opt. Soc. Am. B **5,** 1563–1572 (1988).

12. A. M. Weiner, J. P. Heritage, R. J. Hawkins, R. N. Thurston, E. M. Kirschner, D. E. Leaird, and W. J. Tomlinson, "Experimental observation of the fundamental dark soliton in optical fibers," Phys. Rev. Lett. **61,** 2445–2448 (1988).
13. A. M. Weiner, D. E. Leaird, G. P. Wiederrecht, and K. A. Nelson, "Femtosecond pulse sequences used for optical manipulation of molecular motion," Science **247,** 1317–1319 (1990); "Femtosecond multiple-pulse impulsive stimulated Raman scattering spectroscopy," J. Opt. Soc. Am. B **8,** 1264–1275 (1991).
14. A. M. Weiner and D. E. Leaird, "Generation of terahertz-rate trains of femtosecond pulses by phase-only filtering," Opt. Lett. **15,** 51–53 (1990).
15. J. A. Valdmanis, R. L. Fork, and J. P. Gordon, "Generation of optical pulses as short as 27 femtoseconds directly from a laser balancing self-phase modulation, group velocity dispersion, saturable absorption, and saturable gain," Opt. Lett. **10,** 131–133 (1985).
16. C. Froehly, B. Colombeau, and M. Vampouille, "Shaping and analysis of picosecond light pulses," in *Progress in Optics XX,* E. Wolf, ed. (North-Holland, Amsterdam, 1983), pp. 65–153.
17. A. VanderLugt, "Signal detection by complex spatial filtering," IEEE Trans. Inf. Theory **IT-10,** 139–145 (1964).
18. R. N. Thurston, J. P. Heritage, A. M. Weiner, and W. J. Tomlinson, "Analysis of picosecond pulse shape synthesis by spatial masking in a grating pulse compressor," IEEE J. Quantum Electron. **22,** 682–696 (1986).
19. A. M. Weiner, J. P. Heritage, and J. A. Salehi, "Encoding and decoding of femtosecond pulses," Opt. Lett. **13,** 300–302 (1988).
20. A. M. Weiner, D. E. Leaird, J. S. Patel, and J. R. Wullert, "Programmable femtosecond pulse shaping by use of a multielement liquid-crystal phase modulator," Opt. Lett. **15,** 326–328 (1990).
21. A. M. Weiner, D. E. Leaird, J. S. Patel, and J. R. Wullert, "Programmable shaping of femtosecond optical pulses by use of a 128-element liquid crystal phase modulator," IEEE J. Quantum Electron. **28,** 908–920 (1992).
22. A. M. Weiner, J. P. Heritage, and R. N. Thurston, "Synthesis of phase-coherent, picosecond optical square pulses," Opt. Lett. **11,** 153–155 (1986).
23. K. Ema and F. Shimizu, "Optical pulse shaping using a Fourier-transformed hologram," Jpn. J. Appl. Phys. **29,** L631–L633 (1990).
24. A. M. Weiner, D. E. Leaird, D. H. Reitze, and E. G. Paek, "Spectral holography of shaped femtosecond pulses," Opt. Lett. **17,** 224–226 (1992).
25. R. Skaug and J. F. Hjelmstad, *Spread Spectrum in Communications* (Peregrinus, London, 1985).
26. D. H. Reitze, A. M. Weiner, and D. E. Leaird, "Shaping of wide-bandwidth, 20 femtosecond optical pulses," Appl. Phys. Lett. **61,** 1260–1262 (1992).
27. N. Metropolis, A. Rosenbluth, M. Rosenbluth, A. H. Teller, and E. Teller, "Equation of state calculations by fast computing machines," J. Chem. Phys. **21,** 1087–1092 (1953).
28. S. Kirkpatrick, C. D. Gelatt, and M. P. Vecchi, "Optimization by simulated annealing," Science **220,** 671–680 (1983).
29. W. H. Press, B. P. Flannery, S. A. Teukolsky, and W. T. Vetterling, *Numerical Recipes* (Cambridge U. Press, Cambridge, 1986), pp. 326–334.
30. A. M. Weiner, Y. Silberberg, H. Fouckhardt, D. E. Leaird, M. A. Saifi, M. J. Andrejco, and P. W. Smith, "Use of femtosecond square pulses to avoid pulse breakup in all-optical switching," IEEE J. Quantum Electron. **25,** 2648–2655 (1989).
31. J. L. A. Chilla and O. E. Martinez, "Direct determination of the amplitude and the phase of femtosecond light pulses," Opt. Lett. **16,** 39–41 (1991).
32. D. J. Kane and R. Trebino, "Measurement of the intensity and phase of femtosecond pulses using spectrally resolved self-diffraction," presented at the Eighth International Conference on Ultrafast Phenomena, Juan-Les-Pins, France, June 8–12, 1992.